JACS
JOURNAL OF THE AMERICAN CHEMICAL SOCIETY
Article
pubs.acs.org/JACS

Understanding THz Spectra of Aqueous Solutions: Glycine in Light and Heavy Water

Jian Sun,[†,§] Gudrun Niehues,[‡,⊥] Harald Forbert,[†] Dominique Decka,[‡] Gerhard Schwaab,[‡] Dominik Marx,[†] and Martina Havenith*[,‡]

[†]Lehrstuhl für Theoretische Chemie and [‡]Lehrstuhl für Physikalische Chemie II, Ruhr−Universität Bochum, 44780 Bochum, Germany

Supporting Information

ABSTRACT: THz spectroscopy of aqueous solutions has been established as of recently to be a valuable and complementary experimental tool to provide direct insights into the solute−solvent coupling due to hydrogen-bond dynamics involving interfacial water. Despite much experimental progress, understanding THz spectra in terms of molecular motions, akin to mid-infrared spectra, still remains elusive. Here, using the osmoprotectant glycine as a showcase, we demonstrate how this can be achieved by combining THz absorption spectroscopy and *ab initio* molecular dynamics. The experimental THz spectrum is characterized by broad yet clearly discernible peaks. Based on substantial extensions of available mode-specific decomposition schemes, the experimental spectrum can be reproduced by theory and assigned on an essentially quantitative level. This joint effort reveals an unexpectedly clear picture of the individual contributions of molecular motion to the THz absorption spectrum in terms of distinct modes stemming from intramolecular vibrations, rigid-body-like hindered rotational and translational motion, and specific couplings to interfacial water molecules. The assignment is confirmed by the peak shifts observed in the THz spectrum of deuterated glycine in heavy water, which allow us to separate the distinct modes experimentally.

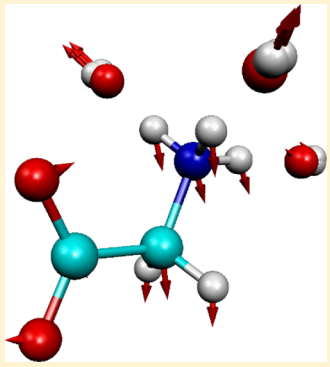

1. INTRODUCTION

Solvation of molecules in water is a core topic in molecular sciences and of broad importance to many subdisciplines within chemistry and biology.[1−7] Based on decades of advances due to spectroscopy in concert with simulation, well-established notions such as interfacial water, solvation water, or so-called "biological water" suggest that the properties of water close to solutes might be vastly different from those known from the bulk liquid. Laser spectroscopy in the frequency window from 1 up to about 5 THz,[8,9] corresponding to roughly 30−200 cm^{-1}, has been proven recently to be a sensitive tool to probe hydration dynamics.[10−19] This is complementary to optical Kerr effect (OKE) spectroscopy that has been employed for a long time to investigate the vibrational dynamics and relaxation processes in water and aqueous solutions.[20−24] Both techniques have been proven to be able to detect the same low-frequency modes describing the rattling modes of ions within their cage.[18,25] Using THz spectroscopy, "extended dynamical hydration shells"[12] have been detected and shown to feature a distinctly different dynamics compared to bulk water.[12,26] Examples of solutes investigated so far in the THz domain range in size and complexity from simple ions[17−19,25,27] to small molecules like carbohydrates,[10,14] amino acids,[28] or urea[29] up to proteins[12,13,15,30,31] and enzymes.[32] The pronounced sensitivity of THz spectroscopy to the dynamics of interfacial water is a consequence of a wealth of dynamical processes, such as hydrogen-bond (HB) rearrangements and rotational relaxation, that constantly take place in the HB network surrounding solutes. These processes, being at the heart of solvation, occur typically on the picosecond time scale, which translates directly into frequencies in the THz range.

Irrespective of these experimental advances, understanding or even assigning THz spectra of aqueous solutions, where resonances are typically broader and weaker compared to the intramolecular vibrations found in the mid-infrared range, is much less developed beyond providing qualitative arguments. Molecular dynamics simulations based on force fields (FFMD) have been used for a long time to compute the vibrational density of states (VDOS) of complex liquids such as proteins in water, including the low-frequency regime that is relevant to THz spectroscopy, see e.g. refs 27 and 33−35 for recent work along these lines and for pointers to the vast earlier literature. The VDOS, however, exclusively probes the correlated motion due to the time evolution of all individual atoms that are contained in the sample, whereas THz spectroscopy measures the correlations in the time evolution of the corresponding total dipole moment. This implies that VDOS intensities can neither be compared to THz or infrared (IR) intensities nor to the corresponding spectral line shapes. Going a step beyond, the total dipole moment can be computed in terms of force field parameters such as partial charges, higher multipole moments, or polarizabilities in conjunction with using classical electrostatics. Following such ideas, the THz line shape of pure bulk

Received: December 20, 2013
Published: March 10, 2014

   dx.doi.org/10.1021/ja4129857 | *J. Am. Chem. Soc.* 2014, 136, 5031−5038

water, in particular the 200 cm^{-1} intermolecular HB network mode, has been reproduced based on a parametrized post-processing of FFMD trajectories.[36]

In contrast to FFMD, *ab initio* molecular dynamics (AIMD)[37] allows one to compute the total dipole moment, and thus the line shape function, directly from the underlying quantum-mechanical electronic structure, which is available "on the fly" in these approaches anyway. Indeed, AIMD simulations have been most successful to decompose IR spectra[38] of solutions into molecular contributions, see e.g. refs 39−46 for a severely incomplete list. Yet, despite much progress on understanding the THz response of simple ions in water,[17−19,25,27] the assignment of THz spectra of even small molecules in aqueous solution remains a challenge. A first step in this direction has been taken recently by dissecting the THz spectrum of the solvent itself, bulk water at ambient conditions, in terms of distinct intermolecular HB network modes based on AIMD trajectories.[47,48] THz spectra of molecules in water, however, are obviously much more complex than those of the neat solvent or solvated simple ions.

The current understanding is that protein and enzyme function is strongly affected by the presence not only of solvent but also by an arsenal of small cosolute molecules. Amino acids, being well-known compatible solutes, act as osmolytes and are thus an important ingredient in cell function. Moreover, they are the basic building blocks of proteins such that it is essential to characterize their hydration dynamics in order to get a picture of the inhomogeneous hydration of proteins. Being zwitterions at physiological conditions, they feature both anionic and cationic solvation shells, being characteristic from biomolecules to polyelectrolytes to fuel cell membranes, in addition to hydrophobic solvation which can be tuned via their side chains. Furthermore, the $-COO^-$ and $-NH_3^+$ groups separated in space create a pronounced molecular dipole moment that is expected to couple well to a polar solvent such as water. The vibrational spectra of amino acids, in particular of glycine as the simplest one, have been studied thoroughly using a broad range of experimental[28,49−52] and theoretical[53−57] approaches. For glycine in water, for instance, it could be shown that perturbations of the geometric and electronic structure of the solvating water molecules are astonishingly small even in the first shell compared to bulk water.[57]

In what follows we will address the problem of determining and understanding the line shape of the low-frequency vibrational response of glycine in water, Gly(aq), by measuring, computing, and assigning its THz spectrum in terms of the correlated dynamics of solute and solvent molecules. Using isotopic substitution in liquid-state THz spectroscopy, the line shape of deuterated glycine in heavy water, $GlyD_3$(aqD), has been measured and is found to change in a very characteristic way that is reproduced by simulation, thus confirming the mode assignment extracted for Gly(aq).

2. METHODS

Normal glycine in buffer solution, Gly(aq), and deuterated glycine-N,N,O-d_3 dissolved in heavy water, $GlyD_3$(aqD), were measured at different concentrations using a wideband Fourier transform (FT) spectrometer. The Gly(aq) solution was additionaly investigated with our narrowband p-Ge laser THz difference spectrometer,[16] see Supporting Information (SI) for details. In the following 'solvent' refers to 50 mM TrisHCl buffer or D_2O in case of Gly(aq) and $GlyD_3$(aqD), respectively. After determination of the effective concentration $c_{solvent}(c)$ for a given solute concentration c by density measurement, we could determine the partial absorption coefficient using

$$\alpha_{part}(\omega, c) = \alpha_{sample}(\omega, c) - \frac{c_{solvent}(c)}{c_0}\alpha_{solvent}(\omega) \quad (1)$$

where c_0 is the concentration of the neat solvent in moles per dm^3.

The computation of total vibrational spectra of aqueous solutions has made lively progress in the past decade. However, the analysis of such spectra, i.e., the assignment of vibrational bands to atomic motions, is by no means straightforward when it comes to low-frequency modes including their strong coupling to solvation shell dynamics, both being crucial to understand measured THz spectra of aqueous solutions. Important steps were the idea to impose a localization criterion in the frequency domain to define "effective modes"[43,44] followed by the introduction of so-called "generalized normal coordinates" that allow one to include large-amplitude motion, permutational symmetries, and different conformations.[58,59]

Here, we generalize these ideas significantly, see SI for background and details, which enables us to investigate the individual contributions of correlated atomic motion to the IR reponse of aqueous solutions down to the low-frequency regime and thus to assign THz spectra. A first step is to include n specific interfacial water molecules, which define what we call a "supermolecular solvation complex" (SSC), denoted in the following as Gly(n H_2O), out of all N water molecules in the sample. Within this framework, it is possible to introduce different SSC models in order to analyze distinct solvation properties. Most of the subsequent analysis is based on the Gly(3 H_2O) SSC, which fully solvates the $-NH_3^+$ group using three water molecules, whereas the contribution due to solvation of the $-COO^-$ group is obtained from considering the Gly(1 H_2O) model, *vide infra*. It is important to realize that such SSC models, including the associated supermolecular dipole moments computed from the electronic structure via Wannier analysis, are exclusively introduced to analyze the trajectories of the solution, in distinct difference to any microsolvation or continuum approach.

Second, the total IR absorption is formulated as a sum over mode-specific absorption coefficients $\alpha_k(\omega)$ and a remaining term describing the off-diagonal correlations,

$$\alpha(\omega) = \sum_k \alpha_k(\omega) + \alpha_{cross}(\omega) \quad (2)$$

as detailed in the SI. Most importantly, the total absorption cross section of the aqueous solution can be recovered systematically by this approach upon summing up the IR contributions of all the individual modes, $\alpha_k(\omega)$. This technique allows us, in particular, to include also selected solvent degrees of freedom and thus intermolecular motion, namely the three water molecules that are strongly hydrogen bonded to the protonated amino group of zwitterionic glycine in the present case. "Synthesizing" the THz spectra step-by-step, i.e., adding the frequency-dependent intensity contribution of one mode after the other, turns out to be a systematic approach to reconstruct the line shape and to come to an assignment of the observed THz absorption features of Gly(aq).

Finally, we can base a mode-specific kinetic energy decomposition scheme on this formalism in order to quantify the relative contributions of hindered translations, rotations,

dx.doi.org/10.1021/ja4129857 | J. Am. Chem. Soc. 2014, 136, 5031−5038

and vibrations of the entire SSC and its fragments, i.e., solvent and solute molecules, to particular THz modes. The total kinetic energy of a particular mode k of the entire SSC, $E_{tot} = \sum_{i\xi} m_i v_{i\xi}^2/2$, is modeled using velocities $v_{i\xi}$ given by the corresponding THz mode vector (see SI for details). The total sum can be split into contributions by water molecules ("Water") and solute in the SSC, and the solute modes can furthermore be decomposed into a center-of-mass part corresponding to hindered translations ("Gly-CoM"), rigid-body-like hindered rotations ("Gly-Rot"), and the intramolecular vibrations ("Gly-Vib") as defined in the SI.

3. RESULTS AND DISCUSSION

3.1. THz Spectra of Glycine in Water. We define the THz contribution due to the solvated amino acids according to eq 1. Based on the wideband measurements, the resulting partial THz absorption coefficient α_{part} for several concentrations of amino acids ranging from 0.4 to 1.8 M is shown in Figure 1A in the full frequency range that is accessible experimentally. Previously, the same procedure was used to determine the partial ionic THz absorption of solvated atomic anions and cations. This allowed us to separate the bulk water absorption from specific resonances which could be assigned to rattling modes of simple atomic ions with their hydration cages.[27] In contrast, the difference spectrum of a molecular solute such as Gly(aq) may contain contributions not only from these translational cage modes but also low-frequency intramolecular and coupled solute−solvent modes from the solvated solute. Here, we find that the main absorption features scale linearly with concentration over the full frequency range covered by our measurements. This is most prominently visible when plotting the averaged THz absorption for a given, restricted frequency interval (gray shading) as a function of glycine concentration (inset). This indicates that the dynamical hydration shell is either small, i.e., restricted to the first hydration shell, or that solute contributions are dominating the THz absorption spectrum. Otherwise a nonlinear dependence would be observed, as e.g. found for solvated disaccharides.[10] In addition, the observed linearity indicates that solute aggregation can be neglected. This is in line with previous results from dielectric spectroscopy[60] where no dipole−dipole correlations were detected up to concentrations of 2.6 M. The THz absorption change observed for Gly(aq) in Figure 1A is 1 order of magnitude larger than the nonlinear THz modulation observed for proteins,[12,26] whereas it is comparable to that found for ions,[17−19,25,27] which are known to have a dominating contribution from the rattling modes of the solute with its hydration shell. Based upon the similarity to the solvated salts and the lack of any obvious nonlinear contribution, using the SSC models for theoretical analyses is expected to be a reasonable approximation for Gly(aq). Note that the observed spectral characteristics did not change when glycine was solvated in ultrapure water instead of 50 mM TrisHCl buffer solution (see Figure 1 in the SI for a comparison). In conclusion, the observed spectra are expected to be well represented by simulations of one glycine molecule in neat water.

3.2. Solute Contributions to Total THz Absorption. Next, we compare the measured difference spectra, $\alpha_{part}(\omega, c)$, to the one calculated at c = 1.7 M in the frequency window accessible to experiment. The thick solid line in Figure 1A represents the spectrum of solvated zwitterionic glycine itself, dubbed "Gly-only", as computed from its dipole autocorrelation function, thus excluding all direct contributions from water. Upon comparing to the experimental difference spectrum, both the shoulder (or weak peak at higher concentrations) at around 80 cm^{-1} and the pronounced peak at about 320 cm^{-1} are nicely reproduced by simulation. However, the broad feature between 100 and 300 cm^{-1} with a maximum around 200 cm^{-1} is well exposed in the experimental spectrum, whereas the calculated Gly-only spectrum shows a rather flat line.

As pointed out before, the spectral change of "solvation water" compared to bulk water is effectively included in the experimental spectra depicted in Figure 1A. In contrast, the displayed Gly-only spectrum (magenta solid line) was

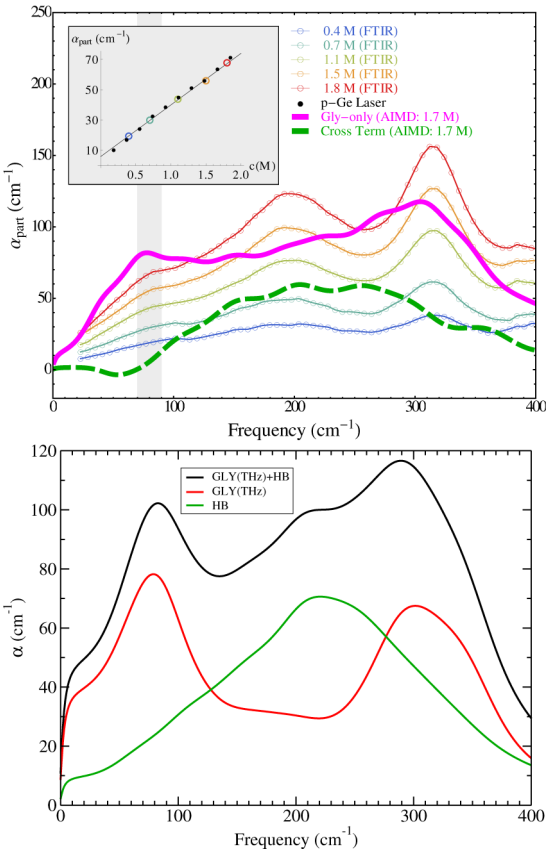

Figure 1. Comparisons between THz measurements and theoretical spectra from AIMD simulations. (A) Top: Partial THz spectra of aqueous glycine for different concentrations as indicated (colored circles). The calculated THz absorption for Gly-only and the total cross-correlation between Gly and all water molecules as obtained from AIMD (see text) are shown as thick solid magenta and dashed green lines, respectively. All AIMD simulations were carried out for a concentration of 1.7 M. The inset shows the good agreement of the wideband FT data averaged over the frequency interval marked by the gray shading (colored dots) to the results for the integrated THz absorption in the same frequency interval (black dots) as measured previously with a precise narrowband p-Ge laser THz difference spectrometer.[28] (B) Bottom: AIMD partial spectra obtained from the supermolecular solvation complexes taking into account only the THz modes (see text for definition). Red line: all modes coming exclusively from glycine motion within Gly(3 H_2O); Green line: all HB modes within Gly(3 H_2O) and scaled HB stretch of Gly(1 H_2O); Black line: sum of red and green partial spectra. These spectra have been obtained as a sum of the respective mode-specific absorption cross sections $\alpha_k(\omega)$ from Figure 2. Note: All computed spectra are shown using otherwise unscaled absolute intensity units as indicated and without adjustment of the frequency scale.

dx.doi.org/10.1021/ja4129857 | J. Am. Chem. Soc. 2014, 136, 5031−5038

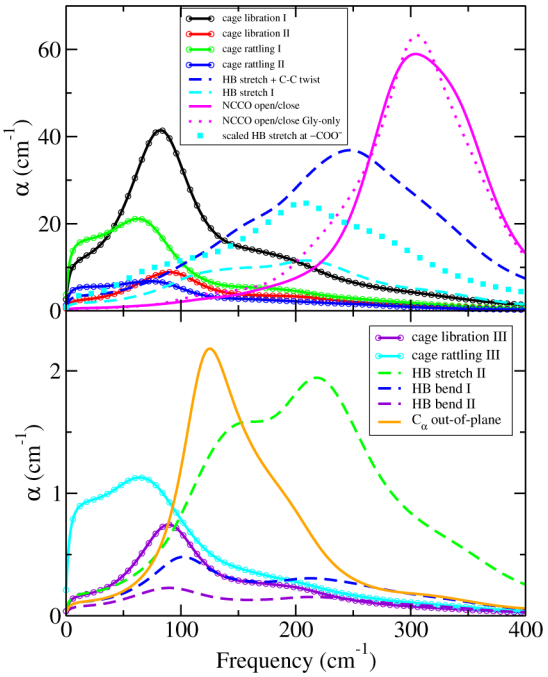

Figure 2. Intensities of THz modes of Gly(aq). All mode-specific absorption cross sections $\alpha_k(\omega)$ of the Gly(3 H_2O) supermolecular solvation complex having intensity maxima below 400 cm^{-1} with high and low absolute intensities are compiled in (A) top and (B) bottom. See labels and text for mode assignments, Figure 3 for corresponding displacement schemes, SI for their dynamical animations, and Table 1 for energy decomposition. The scaled HB stretching mode due to solvation of the $-COO^-$ group (obtained from the Gly(1 H_2O) supermolecular solvation complex, see text and SI) is shown in panel (A) using squares. Note that the dotted line in panel (A) is not obtained from the SSC but the N−C−C−O opening/closing mode of Gly-only.

computed from the dipole moment fluctuations of the solute molecule itself, thus including only the indirect influence of solvation water dynamics on solute dipole dynamics and excluding the changes in the hydration water. This motivated us to investigate in addition the coupling of the glycine fluctuations to those of solvation water in terms of the cross-correlation between the dipole moment of the solute molecule and all water molecules in the simulation box. Remarkably, we find that this solute−solvent cross-term gives rise to a significant absorption feature centered at around 200 cm^{-1}, see green dashed line in Figure 1A, whereas its contribution can be neglected at the two peaks at 80 and 320 cm^{-1}. Thus, the total THz reponse is attributed to the sum of both, the solute itself (Gly-only) and also solute−solvent coupling (cross-correlations). In the following, we will decompose theoretically the THz response of Gly(aq) into contributions of relevant modes by addressing their frequency, intensity, and underlying atomic motions.

3.3. Intramolecular Solute Modes in the THz Domain. As demonstrated by the Gly-only spectrum, the solute molecule itself contributes significantly to the THz response of the solution in important regions of the spectrum, i.e., at 80 and 320 cm^{-1}. But what is the dynamical reason for these modes? To this end our decomposition technique is applied first to disentangle the Gly-only spectrum in terms of the approximately additive mode-specific absorption cross sections $\alpha_k(\omega)$. Only three low-frequency intramolecular modes peaking below 400 cm^{-1} are found, see SI for their dynamical animations. The lowest-frequency such mode with a maximum around 137 cm^{-1} is an out-of-plane motion of the C_α group, followed by a twisting motion of the glycine molecule with respect to its C−C axis at ≈170 cm^{-1} (see Figure 3A). The mode at ≈305 cm^{-1} (see Figure 3B) can be described as closing/opening motion of the N−C−C−O angle, thus involving backbone atoms.

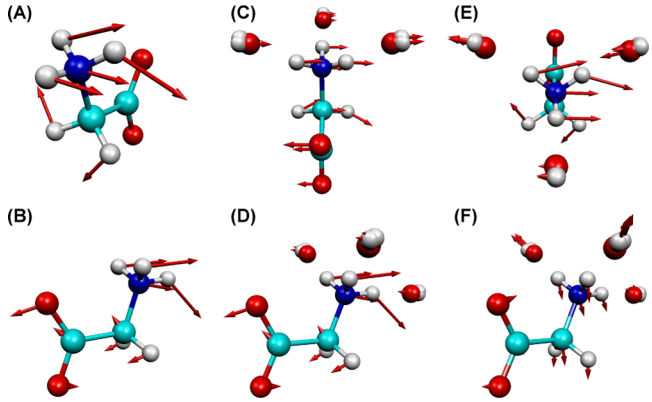

Figure 3. Important THz modes of Gly(aq). All purely intramolecular THz modes of Gly(aq) obtained from the Gly-only spectrum with resonances at (A) 170 cm^{-1} and (B) 305 cm^{-1} corresponding to twisting around the C−C axis and N−C−C−O opening/closing, respectively. Most intense THz modes according to the Gly(3 H_2O) SSC model: (C) libration of quasi-rigid solute ("cage libration I") with a peak maximum at ≈82 cm^{-1} (see SI for the strongest "cage rattling I" mode); (D) glycine opening/closing of the N−C−C−O angle involving backbone atoms ("NCCO open/close") at ≈304 cm^{-1}, (E) HB stretching coupled with C−C twisting ("HB stretch + C−C twist") at ≈247 cm^{-1}, and (F) HB stretching ("HB stretch I") at ≈210 cm^{-1}. The corresponding mode-specific absorption cross sections are depicted in Figure 2A, and dynamical animations for all THz modes are in the SI. The gray, cyan, blue, and red spheres represent the H, C, N, and O atoms, respectively, and the arrows symbolize atom displacements in Cartesian space.

But what about the intensities of these intramolecular modes? The opening/closing motion of the N−C−C−O angle contributes most significantly according to the mode-specific absorption cross sections presented in Figure 2A by the dotted magenta line. Nearly the same result is obtained after adding solvation water, i.e., from analyzing the two SSCs (cf. the solid magenta lines in Figures 2A herein and in the SI). Furthermore, the pronounced intrasolute nature of this mode is clearly supported by the vibrational energy decomposition since $E_{\text{Gly-Vib}}$ > 90% according to Table 1 herein and Table 6 in the SI. In contrast, the other two purely intramolecular THz modes are found to contribute much less to the total intensity.

In summary, a distinct and strictly intramolecular mode of the solvated glycine molecule explains the prominent high-frequency THz absorption band close to 320 cm^{-1} in the experimental spectrum (see Figure 1A), whereas intramolecular motions fail to account for the resonances in the low- and medium-frequency range at about 80 and 200 cm^{-1}, respectively.

3.4. Rigid-Body-Like Solute Motion within the Solvation Cage. In addition to these intrasolute vibrations, it is conceivable that the motion of the solute within its own solvation cage could also contribute to the spectrum at low frequencies. It is known recently that so-called rattling modes

dx.doi.org/10.1021/ja4129857 | J. Am. Chem. Soc. 2014, 136, 5031−5038

Table 1. Decomposition (in percent, deviations from 100% due to rounding) of the Kinetic Energy of the THz Modes of the Gly(3 H_2O) Supermolecular Solvation Complex (see text and SI)

mode according to Figure 2	frequency, cm^{-1}	intensity, cm^{-1}	Gly-CoM	Gly-Rot	Gly-Vib	water
cage rattling I	62	21	85	<1	5	11
cage rattling II	73	7	80	<1	4	15
cage rattling III	64	1	78	<1	2	19
cage libration I	82	41	5	74	4	17
cage libration II	90	9	6	68	4	22
cage libration III	89	<1	2	91	4	3
NCCO open/close	304	59	2	1	92	5
C_α out-of-plane	125	2	4	6	75	15
HB stretch + C−C twist	247	37	13	30	20	37
HB stretch I	210	12	9	21	5	66
HB stretch II	218	2	17	4	6	74
HB bend I	102	<1	<1	8	<1	92
HB bend II	90	<1	<1	<1	2	98

(i.e., hindered translations) can give rise to specific THz absorption bands in the case of simple ions.[18,25,27] But can this sort of motion also be relevant for complex molecules? Indeed, applying our technique to the two SSC models reveals not only three rigid-body-like hindered translational modes ("cage rattling") but also three hindered rotational modes ("cage librations") of the quasi-rigid solute molecule (cf. Figure 2 herein and Figure 3 in the SI). The corresponding kinetic energy decomposition in Table 1 convincingly supports the classification into cage rattling and cage libration modes in view of the overriding "Gly-CoM" and "Gly-Rot" contributions, respectively, and only small components due to intrasolute vibrations, "Gly-Vib", and due to HB "Water". Their mode-specific absorption cross sections, in turn, demonstrate that a specific librational mode ("cage libration I", for the intensity see black line with dots in Figure 2A and for a mode description see Figure 3C) together with a distinct rattling mode of about half its strength ("cage rattling I", see green line with dots in Figure 2A and Figure 3A in the SI) contribute significantly to the intensity in the THz window with peaks at ≈82 and 62 cm^{-1}, respectively. Incidentally, these are the only solvated solute modes that contribute considerably in the range of the low-frequency feature observed in the experimental spectrum, cf. Figure 1A. Importantly, identical analyses of the Gly(1 H_2O) model confirm this picture as seen by comparing to the respective $\alpha_k(\omega)$ spectra and kinetic energy decompositions in the SI (cf. Figure 3 and Table 6 therein).

We conclude at this stage that the low-frequency resonance observed in the spectrum around 80 cm^{-1} can be assigned to essentially rigid-body-like librational and rattling motion of glycine in its transient solvation cage. Still, the intensity of the strongest rattling mode is only about half that of the most pronounced libration for solvated glycine. This situation is, of course, distinctly different for the solvated atomic salts, in which case the rattling modes are the only and therefore most prominent contribution in addition to hydration and bulk water contributions.[18,25,27]

3.5. THz Response of Intermolecular Water−Solute Modes. Yet, this rigid-body-like cage motion together with intramolecular glycine THz modes, leading to the red line in Figure 1B, cannot fully explain the shape of the observed THz domain spectrum. This brings us back to the observation of pronounced solute−solvent coupling, i.e., cross-correlations which are strongly peaked around 200 cm^{-1} according to the green line in Figure 1B, that apparently can "fill in" the missing intensity.

In the following, we analyze intermolecular modes that involve both the solute and solvation water molecules. Upon analyzing the spatial distribution function, see Figure 2 in the SI, one finds the solvation shell of the $-NH_3^+$ group to be well-defined, each of the protons donating a HB to a water molecule.[57] Thus, we selected the corresponding $n = 3$ interfacial water molecules attached to $-NH_3^+$ in order to define the Gly(3 H_2O) SSC model. The $-COO^-$ group has roughly four and a half water molecules in the first solvation shell,[57] which are however very unequally spread over three regions close to the two oxygen atoms. Due to reasons given in the SI, the resulting solvation shell of the carboxylate group is ill-defined in the sense of mode analysis. We therefore consider only the most strongly solvating water molecule in terms of the Gly(1 H_2O) model together with an approximate scaling procedure (tested in the SI) to estimate the spectral contribution of the fully solvated $-COO^-$ group.

When explicitly including these particular solvation water molecules in terms of our two SSC models, we are able to find additional well-defined modes in the THz domain (see Figure 2). These involve HB stretching and bending motion, possibly coupled to intramolecular glycine modes, see e.g. Figure 3E,F and the SI for dynamical animations of all THz modes of Gly(3 H_2O). According to both SSCs, the intermolecular HB bending modes lie in a similar frequency range as the rigid-body cage modes, i.e., 60−100 cm^{-1}. In contrast to HB bending, the HB stretching modes are centered around 200 cm^{-1} for both SSC models, which is exactly the range where the dipolar solute−solvent cross-correlations, as shown by the green dashed line in Figure 1A, are most prominent.

Again, the crucial question relates to the intensity of these HB modes. In the Gly(3 H_2O) model, a particular glycine−water HB stretch coupled with C−C twisting motion within the glycine molecule, "HB stretch + C−C twist" peaking at 247 cm^{-1} (see Figure 3E), has by far the largest IR activity, see dashed dark-blue line in Figure 2A. As a result, the purely intrasolute C−C twist from the previous Gly-only analysis gains intensity and also blue-shifts from 170 to ≈247 cm^{-1} as a result of its significant coupling to interfacial water motion in the SSC, which is roughly 40% according to the energy decomposition (see "HB stretch + C−C twist" in Table 1). The intermolecular HB stretching mode at 210 cm^{-1} ("HB stretch I", see Figure 3F and dashed light-blue line in Figure 2A) has a smaller intensity, whereas "HB stretch II" at 218 cm^{-1} and the "HB bend I/II" modes are weaker by an order of magnitude, see Figure 2B, and thus do not contribute significantly to the total THz line shape. Supplementing these intermolecular contributions of the Gly(3 H_2O) model in the THz regime, solvation of the carboxylate group via the Gly(1 H_2O) model contributes significant HB stretching intensity centered close to 200 cm^{-1} (see light-blue squares in Figure 2A and SI for details).

In conclusion, it is mainly solute−solvent HB stretching motion in the first solvation shells of the charged $-NH_3^+$ and $-COO^-$ groups of zwitterionic Gly(aq) that contributes to the cross-correlations (see green dashed line in Figure 1A) peaked around 200 cm^{-1} as demonstrated by the green line in Figure 1B. These specific modes, in turn, generate an intermediate peak around 200 cm^{-1} in the simulated THz spectrum (see

dx.doi.org/10.1021/ja4129857 | J. Am. Chem. Soc. 2014, 136, 5031−5038

black line in Figure 1B) that is observed as a pronounced peak centered at 200 cm^{-1} in the experimental spectrum. Of course, additional intensity gain at ≈200 cm^{-1} stemming from many but less well-defined contributions due to HB stretching of interfacial water molecules in addition to those considered explicitly in the two SSC models is expected.

3.6. Deuteration Effects on THz Spectra. Is there a possibility to scrutinize our theoretical assignment of the three experimental features at roughly 80, 200, and 320 cm^{-1} ? Isotopic substitution certainly is a standard technique in mid-infrared spectroscopy in order to disentangle peaks due to intramolecular motion, whereas it remains largely unexplored in liquid-state THz spectroscopy. To set the stage, we recall that it has been shown earlier that pure H_2O and D_2O have a very similar line shape in the THz regime and, in particular, that they share the same resonance frequency of the HB network mode, cf. the experimental data in Figure 1 of ref 47. Thus, deuteration is not expected to shift the intermolecular solute−solvent HB stretching mode close to 200 cm^{-1}. In stark contrast, isotopic substitution from Gly to $GlyD_3$ is expected to significantly red-shift those modes that have an overwhelmingly intramolecular character. Thus, the closing/opening motion of the N−C−C−O angle, being responsible for the measured peak around 320 cm^{-1} and having 92% intramolecular vibrational character according to our assignment compiled in Table 1, should considerably shift to the red in the THz spectrum of the deuterated solution. Finally, in view of slightly increased moments of inertia of $GlyD_3$ as a result of deuteration, a very small red-shift could be expected for the intense cage libration mode that is responsible for the weak peak close to 80 cm^{-1}.

These qualitative expectations are indeed discovered in the experimental data obtained for the $GlyD_3$(aqD) solutions depicted by the green lines in Figure 4A: We observe no shift of the HB network mode at 200 cm^{-1} and a minor change of the cage libration band with respect to Gly(aq), whereas a clear ≈20 cm^{-1} red-shift of the pronounced N−C−C-O mode is found. The three peak positions are insensitive to changes in concentration. Their intensities increase linearly with concentration akin to the Gly(aq) spectra presented in Figure 1A.

Due to both the full anharmonic mode coupling and thermal HB fluctuations, probing H/D substitution effects on spectra computed from MD cannot be estimated analytically but requires explicit simulations using D masses. In view of the computational effort of AIMD simulations needed to compute reliably low-frequency spectra (as explained in the SI), we carried out FFMD simulations (see SI for details) of the $GlyD_3$(aqD) system and also of Gly(aq) for consistent reference, see Figure 4B. Before proceeding, careful benchmarking of the performance of FFMD for the present purpose is in order. Clearly, the Gly-only spectrum as produced by FFMD (blue line) for the Gly(aq) solution shares the same peak structure as the full AIMD spectrum (dotted magenta line), except for a systematic blue-shift of the N−C−C−O peak to about 350 cm^{-1} and for a significantly reduced spectral density in the 200 cm^{-1} regime according to Figure 4B. The blue-shift obviously is due to the force constant parametrization according to the force field used (see SI), whereas the missing intensity around 200 cm^{-1} can be traced back to missing polarizability contributions. The latter is demonstrated by computing the THz spectrum from the AIMD trajectories, but after replacing the full electronic structure by the same partial point charges (pc) as those used in the force field simulations.

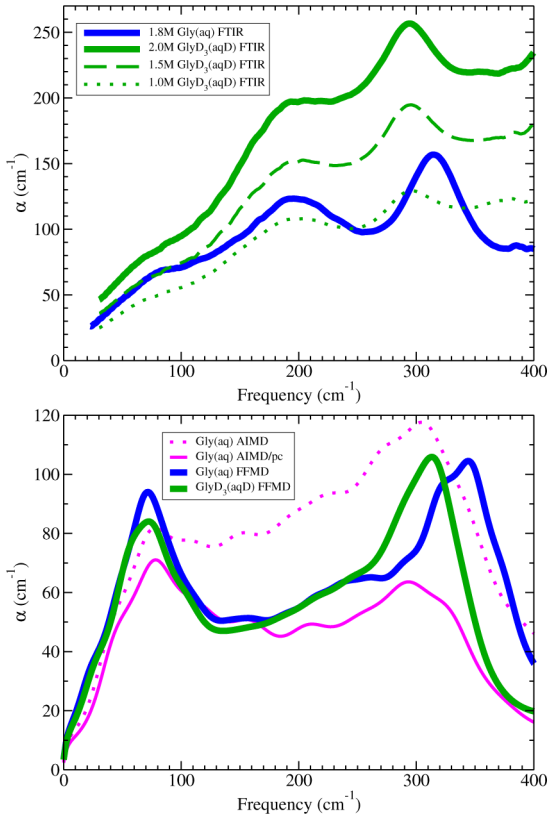

Figure 4. Deuteration effects on solution THz spectra: Gly(aq) versus $GlyD_3$(aqD). (A) Top: Partial THz spectra of $GlyD_3$(aqD) for different concentrations as indicated (green lines) compared to Gly(aq) at 1.8 M (blue line; data reproduced from Figure 1A). (B) Bottom: The calculated THz absorption for Gly-only as obtained from AIMD, AIMD/pc, and FFMD simulations (see text) of Gly(aq) and $GlyD_3$(aqD) as indicated in the caption (the Gly(aq) AIMD data are reproduced from Figure 1A). All MD simulations were carried out for a concentration of 1.7 M, and all computed spectra are shown using otherwise unscaled absolute intensity units as indicated and without adjustment of the frequency scale.

This simplifying AIMD/pc proceedure to compute the dipole moment yields a THz line shape (solid magenta line) in the 200 cm^{-1} frequency regime that comes very close in its low intensity to the one generated by FFMD. Thus, the force field approach does reproduce satisfactorily the experimental resonances at 80 and 320 cm^{-1}. When switching now from Gly(aq) to the deuterated system, $GlyD_3$(aqD), it is observed (green line) that the low-frequency resonance is not affected much, whereas the N−C−C−O peak is seen to clearly red-shift by roughly 30 cm^{-1} in excellent agreement with the experimental observations in the top panel.

In conclusion, the specific deuteration effects observed in the experimental THz spectrum are not only reproduced when simulating the deuterated system but also understood in terms of our mode assignment. Beyond the special case, it appears that isotopic substitution is able to specifically mark and thus to disentangle peaks of largely intramolecular character from others. In summary we propose that deuteration will be a useful technique in future investigations into THz spectra of liquids.

4. CONCLUSIONS AND OUTLOOK

THz spectroscopy as a tool to study (bio)molecular hydration is a rapidly developing field. The focus of this investigation is to

dx.doi.org/10.1021/ja4129857 | J. Am. Chem. Soc. 2014, 136, 5031−5038

understand the measured line shape of the low-frequency vibrational spectrum of a zwitterion solvated in liquid water. This nicely extends our previous studies on cations and anions by providing now a specific mode assignment including solute and solute/solvent coupling terms. Based on a close interplay of theory and experiment we could show that it is possible to assign THz spectra of molecular solutions in terms of atomic motions thus providing a microscopic picture. To this end, the idea of a "supermolecular solvation complex" has been used, where strongly bound interfacial water molecules are explicitly included in the vibrational analysis. For glycine in water studied here, Gly(aq), water molecules solvating the protonated amino and carboxylate groups define the Gly(3 H_2O) and Gly(1 H_2O) SSC models. Introducing in addition a vibrational analysis technique that draws directly on *ab initio* molecular dynamics trajectories the total spectrum $\alpha(\omega)$ can be decomposed into mode-specific absorption cross sections, $\alpha_k(\omega)$, and corresponding atom displacements directly in Cartesian space. In reverse, spectra can be systematically resynthesized using a selected subset $\{\alpha_k(\omega)\}$ of mode-specific contributions, thus probing the importance of specific modes k in terms of their contribution to the absolute IR activity. Moreover, a mode-specific kinetic energy decomposition scheme quantifies to what extent glycine and water fluctuations contribute to specific THz modes.

The analysis techniques introduced here allowed us to unveil three distinct classes of vibrational modes of increasing complexity that are *all* important in the THz regime: (i) essentially purely intramolecular low-frequency modes of the solute itself; (ii) rigid-body-like librational and rattling motion of the molecule in its transient solvation cage; (iii) intermolecular solute−solvent coupling modes due to correlated HB stretching motion, whereas HB bending is shown to be essentially THz silent. Within this general framework, the resulting assignment of the experimental THz spectrum of Gly(aq) turns out to be surprisingly simple: the high-frequency peak at ≈320 cm^{-1} is an intramolecular vibration involving the N−C−C−O angle and thus backbone motions, the lowest-frequency feature around 80 cm^{-1} stems from rigid-body-like librational and also rattling motion of the glycine molecule in its own solvation cage, and the resonance at 200 cm^{-1} is traced back to intermolecular glycine−water HB stretching motion, whereas such bending modes are essentially silent.

Deuteration of both solute and solvent reveals characteristic changes of the THz spectrum. The distinct differences, but also similarities, can be explained by the nature of the three mode families according to our assignment: the intramolecular mode red-shifts significantly, whereas the intermolecular HB stretching modes are unaffected as expected from pure bulk water and the cage mode feature barely changes. These findings demonstrate furthermore that isotopic substitution is expected to be a valuable assignment tool not only in the mid-infrared but also in the THz frequency range.

In conclusion, the line shape of the experimental solution-bulk difference THz spectrum of Gly(aq) emerges as a result of strong intramolecular solute modes interplaying with distinct solute−solvent couplings together with rigid-body-like solute motion within the transient solvation cage. Having shown that such an assignment is possible as a result of a close interplay of experiment and simulation, the developed techniques open up a systematic pathway toward understanding the THz spectra of more complex solvated solutes than glycine, even in other solvents. This might require to exploit the approximate additivity of the THz response of functional groups such as found here for $-NH_3^+$ and $-COO^-$, generalizing spatial decomposition schemes to anisotropic cases and making use of polarizable force fields. As such, experimental and theoretical THz spectroscopy is expected to become one of the key approaches to advance "solvation science" as a coherent field.

■ ASSOCIATED CONTENT

Supporting Information

Experimental details on Fourier transform measurements; computational details; simulation analysis methodologies; solvation details of $-NH_3^+$ versus $-COO^-$ group; animated THz modes of glycine with 3 water molecules; animated THz modes of glycine; $-COO^-$ group contribution estimation; mode character decomposition table. This material is available free of charge via the Internet at http://pubs.acs.org.

■ AUTHOR INFORMATION

Corresponding Author

Martina.Havenith@rub.de

Present Addresses

[§]Department of Physics and National Laboratory of Solid State Microstructures, Nanjing University, Nanjing 210093, China.
[⊥]Research Center for Development of Far-Infrared Region, University of Fukui, Fukui 910-8507, Japan.

Notes

The authors declare no competing financial interest.

■ ACKNOWLEDGMENTS

It is a pleasure to thank Gerald Mathias, Marcel Baer, Maciej Smiechowski, Matthias Heyden, Erik Bründermann, Valeria Conti Nibali, and Stefan Funkner for many fruitful discussions and help. We acknowledge financial support of Alexander von Humboldt Stiftung (Fellowship to J.S.), Deutsche Forschungsgemeinschaft (MA 1547/11), BMBF (05KS7PC2), Volkswagen Stiftung, the Ruhr−Universität Bochum and the Ruhr-University Research School funded by Germany's Excellence Initiative [DFG GSC 98/1], and Ruhr−Universität Bochum. This work is part of the Cluster of Excellence RESOLV (EXC 1069) funded by the Deutsche Forschungsgemeinschaft. The calculations were carried out using resources of SuperMUC@LRZ, Bovilab@RUB, and Rechnerverbund−NRW.

■ REFERENCES

(1) Robinson, G. W.; Zhu, S.-B.; Singh, S.; Evans, M. W. *Water in Biology, Chemistry and Physics: Experimental Overviews and Computational Methodologies*; World Scientific: Singapore, 1996.
(2) Franks, F. *Water: A matrix of Life*, 2nd ed.; Royal Society of Chemistry: Cambridge, 2000.
(3) Bagchi, B. *Chem. Rev.* **2005**, *105*, 3197−3219.
(4) Bakker, H. J. *Chem. Rev.* **2008**, *108*, 1456−1473.
(5) Ball, P. *Chem. Rev.* **2008**, *108*, 74−108.
(6) Laage, D.; Stirnemann, G.; Sterpone, F.; Hynes, J. T. *Acc. Chem. Res.* **2012**, *45*, 53−62.
(7) Bagchi, B. *Water in Biological and Chemical Processes: From Structure and Dynamics to Function*; Cambridge University Press: Cambridge, 2013.
(8) Schmuttenmaer, C.-A. *Chem. Rev.* **2004**, *104*, 1759−1779.
(9) Plusquellic, D. F.; Siegrist, K.; Heilweil, E. J.; Esenturk, O. *ChemPhysChem* **2007**, *8*, 2412−2431.
(10) Heugen, U.; Schwaab, G.; Bründermann, E.; Heyden, M.; Yu, X.; Leitner, D.-M.; Havenith, M. *Proc. Natl. Acad. Sci. U.S.A.* **2006**, *103*, 12301−12306.

(11) Zhang, C.; Durbin, S.-M. *J. Phys. Chem. B* **2006**, *110*, 23607−23613.
(12) Ebbinghaus, S.; Kim, S.-J.; Heyden, M.; Yu, X.; Heugen, U.; Gruebele, M.; Leitner, D.-M.; Havenith, M. *Proc. Natl. Acad. Sci. U.S.A.* **2007**, *104*, 20749−20752.
(13) Ebbinghaus, S.; Kim, S.-J.; Heyden, M.; Yu, X.; Gruebele, M.; Leitner, D.-M.; Havenith, M. *J. Am. Chem. Soc.* **2008**, *130*, 2374−2375.
(14) Heyden, M.; Niehues, G.; Heugen, U.; Leitner, D.-M.; Havenith, M. *J. Am. Chem. Soc.* **2008**, *130*, 5773−5779.
(15) Kim, S.-J.; Born, B.; Havenith, M.; Gruebele, M. *Angew. Chem., Int. Ed.* **2008**, *47*, 6486−6489.
(16) Born, B.; Weingärtner, H.; Bründermann, E.; Havenith, M. *J. Am. Chem. Soc.* **2009**, *131*, 3752−3755.
(17) Tielrooij, K. J.; Garcia-Araez, N.; Bonn, M.; Bakker, H. J. *Science* **2010**, *328*, 1006−1009.
(18) Heisler, I. A.; Meech, S. R. *Science* **2010**, *327*, 857−860.
(19) Tielrooij, K. J.; van der Post, S. T.; Hunger, J.; Bonn, M.; Bakker, H. J. *J. Phys. Chem. B* **2011**, *115*, 12638−12647.
(20) Palese, S.; Schilling, L.; Miller, R. D.; Staver, P. R.; Lotshaw, W. T. *J. Phys. Chem.* **1994**, *98*, 6308−6316.
(21) Castner, E. W.; Chang, Y. J.; Chu, Y. C.; Walrafen, G. E. *J. Chem. Phys.* **1995**, *102*, 653−659.
(22) Mazur, K.; Heisler, I. A.; Meech, S. R. *J. Phys. Chem. B* **2011**, *115*, 2563−2573.
(23) Mazur, K.; Heisler, I. A.; Meech, S. R. *J. Phys. Chem. A* **2012**, *116*, 2678−2685.
(24) Taschin, A.; Bartolini, P.; Eramo, R.; Righini, R.; Torre, R. *Nat. Commun.* **2013**, *4*, 2401.
(25) Schmidt, D. A.; Birer, Ö.; Funkner, S.; Born, B. P.; Gnanasekaran, R.; Schwaab, G. W.; Leitner, D. M.; Havenith, M. *J. Am. Chem. Soc.* **2009**, *131*, 18512−18517.
(26) Ebbinghaus, S.; Meister, K.; Prigozhin, M. B.; DeVries, A. L.; Havenith, M.; Dzubiella, J.; Gruebele, M. *Biophys. J.* **2012**, *103*, L20−L22.
(27) Funkner, S.; Niehues, G.; Schmidt, D. A.; Heyden, M.; Schwaab, G.; Callahan, K. M.; Tobias, D. J.; Havenith, M. *J. Am. Chem. Soc.* **2012**, *134*, 1030−1035.
(28) Niehues, G.; Heyden, M.; Schmidt, D. A.; Havenith, M. *Faraday Discuss.* **2011**, *150*, 193−207.
(29) Funkner, S.; Havenith, M.; Schwaab, G. *J. Phys. Chem. B* **2012**, *116*, 13374−13380.
(30) Vinh, N. Q.; Allen, S. J.; Plaxco, K. W. *J. Am. Chem. Soc.* **2011**, *133*, 8942−8947.
(31) Lipps, F.; Levy, S.; Markelz, A. G. *Phys. Chem. Chem. Phys.* **2012**, *14*, 6375−6381.
(32) Grossman, M.; Born, B.; Heyden, M.; Tworowski, D.; Fields, G. B.; Sagi, I.; Havenith, M. *Nat. Struct. Mol. Biol.* **2011**, *18*, 1102−1108.
(33) Ding, T.; Huber, T.; Middelberg, A. P. J.; Falconer, R. J. *J. Phys. Chem. A* **2011**, *115*, 11559−11565..
(34) Sushko, O.; Dubrovka, R.; Donnan, R. S. *J. Phys. Chem. B* **2013**, *117*, 16486−16492.
(35) Heyden, M.; Tobias, D. J. *Phys. Rev. Lett.* **2013**, *111*, 218101.
(36) Torii, H. *J. Phys. Chem. B* **2011**, *115*, 6636−6643.
(37) Marx, D.; Hutter, J. *Ab Initio Molecular Dynamics: Basic Theory and Advanced Methods*; Cambridge University Press: Cambridge, 2009.
(38) Silvestrelli, P.-L.; Bernasconi, M.; Parrinello, M. *Chem. Phys. Lett.* **1997**, *277*, 478−482.
(39) Gaigeot, M. P.; Sprik, M. J. *J. Phys. Chem. B* **2003**, *107*, 10344−10358.
(40) Gaigeot, M. P.; Vuilleumier, R.; Sprik, M. J.; Borgis, D. *J. Chem. Theory Comput.* **2005**, *1*, 772−789.
(41) Iftimie, R.; Tuckerman, M. E. *J. Chem. Phys.* **2005**, *122*, 214508.
(42) Iftimie, R.; Tuckerman, M. E. *Angew. Chem., Int. Ed.* **2006**, *45*, 1144−1147.
(43) Martinez, M.; Gaigeot, M. P.; Borgis, D.; Vuilleumier, R. *J. Chem. Phys.* **2006**, *125*, 144106.
(44) Gaigeot, M. P.; Martinez, M.; Vuilleumier, R. *Mol. Phys.* **2007**, *105*, 2857−2878.
(45) Gaigeot, M. P. *Phys. Chem. Chem. Phys.* **2010**, *12*, 3336−3359.
(46) VandeVondele, J.; Troester, P.; Tavan, P.; Mathias, G. *J. Phys. Chem. A* **2012**, *116*, 2466−2474.
(47) Heyden, M.; Sun, J.; Funkner, S.; Mathias, G.; Forbert, H.; Havenith, M.; Marx, D. *Proc. Natl. Acad. Sci. U.S.A.* **2010**, *107*, 12068−12073.
(48) Heyden, M.; Sun, J.; Forbert, H.; Mathias, G.; Havenith, M.; Marx, D. *J. Phys. Chem. Lett.* **2012**, *3*, 2135−2140.
(49) Chapo, C. J.; Paul, J. B.; Provencal, R. A.; Roth, K.; Saykally, R. J. *J. Am. Chem. Soc.* **1998**, *120*, 12956−12957.
(50) Ramirez, F.; Tunon, I.; Silla, E. *Chem. Phys.* **2004**, *303*, 85−96.
(51) Jalkanen, K. J.; Degtyarenko, I. M.; Nieminen, R. M.; Cao, X.; Nafie, L. A.; Zhu, F.; Barron, L. D. *Theor. Chem. Acc.* **2008**, *119*, 191−210.
(52) Panuszko, A.; Smiechowski, M.; Stangret, J. *J. Chem. Phys.* **2011**, *134*, 115104.
(53) Alper, J. S.; Dothe, H.; Coker, D. F. *Chem. Phys.* **1991**, *153*, 51−62.
(54) Brancato, G.; Barone, V.; Rega, N. *Theor. Chem. Acc.* **2007**, *117*, 1001−1015.
(55) Kundrat, M. D.; Autschbach, J. *J. Chem. Theory Comput.* **2008**, *4*, 1902−1914.
(56) Chowdhry, B. Z.; Dines, T. J.; Jabeen, S.; Withnall, R. *J. Phys. Chem. A* **2008**, *112*, 1033−10347.
(57) Sun, J.; Bousquet, D.; Forbert, H.; Marx, D. *J. Chem. Phys.* **2010**, *133*, 114508−1-−10.
(58) Mathias, G.; Baer, M. D. *J. Chem. Theory Comput.* **2011**, *7*, 2028−2039.
(59) Mathias, G.; Ivanov, S. D.; Witt, A.; Baer, M. D.; Marx, D. *J. Chem. Theory Comput.* **2012**, *8*, 224−234.
(60) Sato, T.; Buchner, R.; Fernandez, S.; Chiba, A.; Kunz, W. *J. Mol. Liq.* **2005**, *117*, 93−98.